Effect of correlation on viscosity and diffusion in molecular-dynamics simulations

Edmund R. Meyer,[1,*] Joel D. Kress, Lee A. Collins, and Christopher Ticknor
Theoretical Division, Los Alamos National Laboratory, Los Alamos, New Mexico 87545, USA
(Received 29 April 2014; published 6 October 2014)

In the warm dense matter (WDM) regime, material properties like diffusion and viscosity can be obtained from lengthy quantum molecular dynamics simulations, where the quantum behavior of the electrons is represented using either Kohn-Sham or orbital-free density functional theory. To reduce the simulation duration, we fit the time dependence of the autocorrelation functions (ACFs) and then use the fit to find values of the diffusion and viscosity. This fitting procedure avoids noise in the long time behavior of the ACFs. We present a detailed analysis of the functional form used to fit the ACFs, which is always a more efficient means to obtain mass transport properties. We use the fits to estimate the statistical error of the transport properties. We apply this methodology to a dense correlated plasma of copper and a mixture of carbon and hydrogen. Both systems show structure in their ACFs and exhibit multiple time scales. The mixture contains different structural forms of the ACFs for each component in the mixture.

DOI: 10.1103/PhysRevE.90.043101 PACS number(s): 52.25.Fi, 52.65.Yy

I. INTRODUCTION

The warm, dense matter (WDM) regime spans a broad range of phenomena and conditions from solids around melt to high-density, high-temperature plasmas. Earth-based examples include many high-energy density physics experiments such as inertial confinement fusion [1] and laser-shocks [2] while those extraterrestrial encompass stellar atmospheres and planetary interiors such as ice giants like Neptune and Uranus [3,4] as well as exoplanets [5,6]. These diverse environments consist of complex mixtures of an eclectic blend of ions, atoms, and light electrons, which exhibit correlated liquid-like behavior that can involve transient molecular formations at the lower temperatures. The modeling and characterization of these systems depend on various microscopic properties, in particular diffusion and viscosity. To understand these processes, we examine their transport properties with quantum molecular dynamics simulations via various autocorrelation functions (ACFs). We find diffusion and viscosity from the long time value of the integrated velocity (VACF) and stress tensor (STACF) ACFs. Even in classical MD, these ACFs exhibit structure that details the behavior and correlation of the particles. Noise from statistical sampling in the late time behavior of the ACFs leads to fluctuations, which makes it difficult to accurately obtain results from the integrated ACFs, especially when the system has correlated time behavior. In classical MD, this can be overcome by using long simulation times.

However, in the WDM regime classical MD does not generically represent all the physics. To most efficiently incorporate the electronic contribution, we use a Thomas-Fermi-Dirac theory for electronic structure coupled with classical MD motion of the ions, commonly called orbital free molecular dynamics (OFMD). Yet this method is computationally costly and thus prohibits long simulation durations, particularly in the case of mixtures of ions requiring larger total particle number. To avoid this obstacle, one can use functions that describe the temporal behavior of the ACFs. These functions are physically motivated from dense liquid theory and include structure in the ACFs. Then the long time behavior of the integrated functional form yields the desired transport property.

In previous works [7–9] a simple, single exponential (or Gaussian) model was used to fit the VACF and STACF. This provided minimal fitting properties and a direct physical interpretation of the constant in the exponential. The motivation of this fitting scheme is based on the Enskog hard-sphere result where the VACF decays exponentially in time [10,11]. In the weakly interacting limit, this assumption is quite good and produces accurate results [7–9].

Reference [12] noted that a single exponential function might not lead to the correct diffusion and viscosity parameters. This is true for the cases analyzed, where the systems were always strongly coupled. The plasma parameter Γ, which measures the coupling strength, is given by

$$\Gamma_{ij} = Z_i^* Z_j^* / (r_s k_B T_{\text{ion}}), \tag{1}$$

where Z_i^* is the effective charge of the ith ion, r_s is the single ion sphere radius, and T is the temperature. When Γ_{ij} is large, the system is in the strongly interacting limit, and the motion of the ions will be correlated. One example in Ref. [12] is Copper (Cu) at a temperature of $T = 100$ eV and a density of $\rho = 67.4\ \text{g/cm}^3$, which gives $\Gamma = 24$. (The authors in Ref. [12] used the value $\Gamma = 167$, but this uses the full atomic Z and not the effective charge that the Cu ions would have in the hot, dense plasma.) This is such a strongly coupled regime that we expect correlated behavior as well as structure in both the VACF and STACF. A conclusion drawn from these examples was the need to use long simulations to arrive at the true values for the properties, especially for viscosity [12]. Such simulations were done with a small number of particles to reduce computational demand. However, in many instances large particle numbers might be necessary, and therefore accuracy in the simulations will be sacrificed because long simulation runs are not feasible.

We further explore ACFs when more than one ion species is present. A complication for multiple ion mixtures is the lack of a unique Γ in that Γ_{ij} depends on which two sample ions are considered. For a CH mixture at $T = 10$ eV with a density (ρ) of 1 and 16 g/cm^3, we estimate $\Gamma_{\text{HH}} = 0.5$ and 2, $\Gamma_{\text{HC}} = 1.2$ and 8, and $\Gamma_{\text{CC}} = 3.0$ and 24, respectively, using the methods of Ref. [13]. Even for this relatively simple example,

*meyer@lanl.gov

many different physical processes (coupling strengths) occur. Generally, the higher Z material, in this case C, will be more strongly interacting and will exhibit more correlated behavior. However, the mixed interactions between low and high Z will be more correlated than the low Z alone. This variety of behavior leads to multiple times scales in the ACFs.

In this paper, we develop and systematically study a fitting procedure for ACFs to improve the accuracy and improve the computational efficiency of obtaining the transport properties. We derive a fitting form with multiple times scales, extending the work of Refs. [14,15]. This physically motivated form can then be used to fit correlated systems and mixtures which exhibit multiple times scales. We study the error of the transport properties from simulations. We show the fitting procedure can be used to save time and understand the form of the ACFs. Additionally, we study a CH mixture, relevant to inertially confined fusion systems, and find that the mixture nature of the system adds complex time dependence to the ACFs. Reference [12] raises issues with using a single exponential fit to the ACFs in correlated simulations. We address these issues with the multitime scale functional forms found here. Reference [12] was able to extract an accurate STACF with small numbers of particles and simulations running for long durations. This strategy may not be possible for mixtures because in order to achieve statistical sampling of all constituents a large total particle number is required. The ultimate intention of this work is to study how to extract transport properties from correlated systems and mixtures. We do not seek to study the mixtures themselves, as many others have done this, for example, Refs. [16–18]. Rather this work serves as a presentation of methods, which we will then apply to more complex, multicomponent mixtures.

II. FORMULATION

A. OFMD methods

We use OFMD as the basis for our studies of Cu and CH at various temperatures and densities. We start with a cubic volume $V = L^3$, with L the side length, that has a particular number of atoms N_i with mass m_i yielding a density $\rho = \sum_i m_i N_i / V$. Individual concentrations are given by the molar fraction $x_i = N_i / N_{\text{tot}}$. The kinetic energy is considered in a semiclassical approximation to first order in the partition function of the electrons. The orbital-free procedure treats all electrons equally and makes no distinction between bound and ionized electrons.

Calculating the orbital-free electronic energy at ion position $\mathbf{R}$ is given by

$$F_e[\mathbf{R},n_e] = \frac{1}{\beta}\int d\mathbf{r} n_e(\mathbf{r})\Phi[n_e(\mathbf{r})] - \frac{2\sqrt{2}}{3\pi^2\beta^{\frac{5}{2}}}\int d\mathbf{r}\, I_{\frac{3}{2}}\{\Phi[n_e(\mathbf{r})]\} + \int d\,\mathbf{r} V_{\text{ext}}(\mathbf{r}) + \frac{1}{2}\iint d\,\mathbf{r}\, d\,\mathbf{r}' \frac{n_e(\mathbf{r})n_e(\mathbf{r}')}{|\mathbf{r}-\mathbf{r}'|} + F_{xc}[n_e], \quad (2)$$

with $\beta = 1/k_B T$, T the temperature, k_B the Boltzmann constant, and I_ν the Fermi integral of order ν. The electrostatic screening potential $\Phi[n_e(\mathbf{r})]$ is related to the electronic density $n_e(\mathbf{r})$ by [19]

$$\nabla^2\Phi[n_e(\mathbf{r})] = 4\pi n_e(\mathbf{r}) = \frac{4\sqrt{2}}{\pi^2\beta^{\frac{3}{2}}} I_{\frac{1}{2}}\{\Phi[n_e(\mathbf{r})]\}, \quad (3)$$

with conservation of charge requiring the integral $\int d\,\mathbf{r} n_e(\mathbf{r})$ to equal the total electronic charge. The first term in Eq. (2) is the finite temperature Thomas-Fermi expression [20]. Other terms represent the Hartree contribution to the electronic energy, the external or electron-ion interaction, and the exchange-correlation potential. We express this last term in the local density approximation of Perdew and Zunger [21,22]. We omit the von Weiszäcker correction and work in a Thomas-Fermi-Dirac form using the formula developed by Perrot [23] to represent the kinetic-entropic piece. We regularized the ionic potential as done in Refs. [24–26] using a radial cut off of $0.3\,a_B$.

At every time step the electronic energy is minimized in terms of the local electronic density for a set of ion positions. Then the forces acting on each ion due to this electronic density are calculated, and the ions are then propagated classically according to this electronic force as well as the ion-ion repulsion. We assume local thermodynamic equilibrium (LTE), which means the electronic and ionic temperatures are the same. In our simulations we fix the electron temperature and use an isokinetic thermostat applied to each ion species [27].

Our static and transport properties such as pressure and diffusion are calculated in the usual manner [28–30]. The total pressure P is given by a sum of the ideal gas pressure of the ions and the electron pressure P_e,

$$P = nk_B T + P_e, \quad (4)$$

with $n = N/V$ the number density. P_e is computed from the electronic forces from the DFT calculation and averaged over the portion of the trajectory that represents equilibration.

The self-diffusion coefficient D_i is given for species i in terms of either the mean square displacement or the integral of the velocity autocorrelation function. For the latter,

$$D_i = \lim_{t\to\infty} \bar{D}_i(t), \quad (5)$$

$$\bar{D}_i(t) = \frac{1}{3}\int_0^t d\,t' \langle \mathbf{v}_j(t')\cdot\mathbf{v}_j(0)\rangle, \quad (6)$$

where $\mathbf{v}_j(t)$ is the velocity of the jth particle of species i, and the brackets represent an ensemble average.

Viscosity is computed from the autocorrelation of the off-diagonal component of the stress tensor [28],

$$\eta = \lim_{t\to\infty} \bar{\eta}(t), \quad (7)$$

$$\bar{\eta}(t) = \frac{V}{k_B T}\int_0^t d\,t' \langle s_{ij}(t')\, s_{ij}(0)\rangle, \quad (8)$$

where $s_{ij}(t)$ is a particular component of the stress tensor at time t. (The stress tensor is the negative of the pressure tensor.) This is a global property that does not benefit from more particles in the simulation. To gather better statistics, we averaged the results of the five independent off-diagonal components of the stress tensor $s_{xy}, s_{yz}, s_{zx}, (s_{xx}-s_{yy})/2$, and $(s_{yy}-s_{zz})/2$.

We also use pair distribution functions (PDFs) to determine the role that structure may play. The PDF is given by

$$g_{ab}(r) = \frac{1}{N_a N_b} \sum_{i=1}^{N_a} \sum_{j=1}^{N_b} \langle \delta(|\mathbf{r}_i - \mathbf{r}_j| - r) \rangle \tag{9}$$

and is an ensemble average. For a completely noninteracting system of hard spheres, the value of $g(r)$ is unity beyond the single ion sphere radius. However, when interactions become important, peaks and valleys emerge in the $g(r)$, indicating the presence of structure in the system.

B. Autocorrelation functions

Studies of correlated liquids have shown that a single exponential function will not adequately describe the diffusive properties of a dense system [31]. There are many techniques for incorporating more physics into the fit of the VACF. One such technique is the continued fraction method for the memory kernel, where by keeping successive orders in the continued fraction one arrives at ever more intricate expressions for the VACF [31,32]. At third order, and for low frequency oscillations, the VACF is given by [31]

$$\langle \mathbf{v}(t) \cdot \mathbf{v}(0) \rangle = a_0 e^{-t/\tau_0} + a_1 e^{-t/\tau_1} [\cos(\omega_1 t) + \alpha_1 \sin(\omega_1 t)], \tag{10}$$

where $\mathbf{v}(t)$ is the velocity at time t, τ_0 and τ_1 are decay times, and ω_1 describes the frequency of collective motion (or restorative forces) near the onset of solidification. (One can derive this expression by using the itinerant oscillator model of Sears [14], for which a generalization to multicomponent is given in the Appendix.) We constrain the parameter α_1 by imposing the property of VACF that the first time-derivative be zero at $t = 0$ vary freely. Additionally, the sum of a_0 and a_1 (the $t = 0$ value of the VACF) is related to the mass of the species and temperature and thus provides a second constraint. Physically, as solidification occurs, the relative ratio of a_0 to a_1 must go from $a_0/a_1 \gg 1$ to $a_0/a_1 \ll 1$. In fact, $a_0 \to 0$ corresponds to the second-order limit of the continued fraction approach to the memory function [31,32]. Using Eq. (6) we immediately find the diffusion constant

$$D = a_0\tau_0 + a_1\tau_1 \frac{1 + \alpha_1\tau_1\omega_1}{1 + \tau_1^2\omega_1^2}. \tag{11}$$

In Eq. (10), the result is derived for a single species. Yet, in a mixture, there can be multiple restoring forces or multiple frequencies of collective motion, acting on a given ion because there are multiple interacting species. For fitting purposes, it may prove requisite to allow for multiple restoring forces. Thus, in the binary fluid one might expect not one but two such forces for each species. For our example, C-C and C-H forces will affect the VACF for C. In that regard, a more general fitting function is

$$\langle \mathbf{v}(t) \cdot \mathbf{v}(0) \rangle = a_0 e^{-t/\tau_0} + \sum_{i=1}^{j} a_i e^{-t/\tau_i} [\cos(\omega_i t) + \alpha_i \sin(\omega_i t)], \tag{12}$$

where j is the number of restoring-type forces included. A sketch of the derivation is in the Appendix. The first term describes hard-sphere-like motion while the secondary terms represent the correlated motions present in the system. Applying Eq. (6) to Eq. (12) yields the diffusion constant

$$D = a_0\tau_0 + \sum_{i=1}^{j} a_i\tau_i \frac{1 + \alpha_i\tau_i\omega_i}{1 + \tau_i^2\omega_i^2}. \tag{13}$$

We use a nonlinear least-squares fit to the VACF with the functional form in Eq. (12) and then extract the value of the diffusion constant using Eqs. (11) and (13). A pure exponential fit is performed setting $a_i = 0 \; \forall \; i > 0$ for comparisons to the older fit model [7–9]. Aside from the error associated with each fitting parameter, we also need to know the error due to statistics built up over the course of a simulation run.

For a single exponential, the idealized statistical error is defined in the limit that the $t_w \to \infty$, where t_w is time window, and it is the duration over which the ACFs are analyzed. In this case, the error is [28,33]

$$\mathcal{E} = \sqrt{\frac{2\tau}{N_i \, T_{\text{traj}}}}, \tag{14}$$

where T_{traj} is the total trajectory time, τ the single decay time, and N_i the number of particles of species i in the simulation. For bulk properties such as viscosity, $N = 1$ because there is only one system. Therefore, we can get strong statistical convergence in the diffusive properties, but not necessarily in the viscosity, for a given T_{traj}. This is in contrast to Ref. [12], where (1) the diffusive and viscous properties are obtained from different simulations and (2) a t_w half the size of the T_{traj}. By using such a large t_w other statistical errors can creep in associated with a nonneglible fraction t_w/T_{traj}.

The statistical inefficiency [28] is dependent on t_w, where $Mt_w = T_{\text{traj}}$ and M is the number of windows sampled in the simulation. If t_w is too large, then the extracted ACF will have additional noise in the regime $t \leqslant t_w$. (Likewise if t_w is too small then the decay time τ will be poorly fitted.) This noise is due to the fact that as the correlation function approaches the intrinsic value at t, the correlated value will take random walks away from the true value. Therefore, as t_w gets larger and larger, the spread about the true value will increase, at roughly a $\sqrt{t_w/T_{\text{traj}}}$ spread. But, t_w must be large enough to capture the longest decay time, τ, of the system. Therefore, we require at minimum $\tau < t_w \ll T_{\text{traj}}$. Because we have multiple time scales, we require

$$t_w > c_0\tau_0 + \sum_{i=1}^{j} c_i\tau_i \frac{1 + \alpha_i\tau_i\omega_i}{1 + \tau_i^2\omega_i^2}, \tag{15}$$

where the c_i are the relative weights of the a_i, $c_i = a_i / \sum_i a_i$. We can think of the weighted sum as being an average, effective decay time. Yet, to accurately fit the longest decay time requires $t_w > \text{Max}[\tau_i]$, and thus this is our criterion for the correct t_w to use in the analysis of the data.

In a manner similar to deriving Eq. (14), we can write down the idealized statistical error for Eqs. (10) and (12) as

$$\mathcal{E} = \sqrt{\frac{2}{N T_{\text{traj}}} \left(c_0\tau_0 + \sum_{i=1}^{j} c_i\tau_i \frac{1 + \alpha_i\tau_i\omega_i}{1 + \tau_i^2\omega_i^2} \right)}. \tag{16}$$

It is evident that the relative weight of each time scale is important as are the restoring force parameters ω_i. We note that the parameters a_i and α_i in Eqs. (10) and (12) are not independent of each other, as mentioned before. With multiple α_i we constrain one of them by requiring that the first time-derivative of the VACF be zero at $t = 0$. We also constrain one a_i such that the normalized VACF be unity at $t = 0$. As solidification becomes dominant ($\tau_i\omega_i \gg 1$) the number of particles freely diffusing will also tend toward zero. Therefore, a_0 will tend toward zero as well, thereby decreasing its importance in the error estimate.

Systems that display multiple decay times in the VACF often have multiple decay times in the STACF. One known method for describing viscosity in these systems is to use a Kohlrausch law [34]. In previous studies of liquids near a triple point, a two-exponential fit was used to describe the VACF [35]. A two-exponential fit is a limit of the general Kohlrausch law which is given by

$$\langle \mathbf{s}(t)\cdot\mathbf{s}(0)\rangle = b_0 e^{-(t/\tau_0)^{\beta_0}} + b_1 e^{-(t/\tau_1)^{\beta_1}}\cos(\omega_1 t), \quad (17)$$

where $\mathbf{s}(t)$ is the stress-tensor at time t. It is often convenient to use $\beta_i = 1$, $\beta_i = 2$, or a combination when fitting the two time-scale STACF. In this paper we will solely use $\beta_i = 1$ or 2 and do not allow the parameter to vary. The presence of ω_1 is again attributable to some form of structure occurring in the system. Using Eq. (8) we find the analytic expression when $\beta_i = 1$:

$$\bar{\eta}(t) = b_0\tau_0 + \frac{b_1\tau_1}{1+(\tau_1\omega_1)^2}. \quad (18)$$

The methods applied to analyze statistical error in the VACF can be applied to the STACF. The integrals simplify for $\beta_i = 1$ or $\beta_i = 2$. For $\beta_i = 1$ the idealized error is

$$\mathcal{E} = \sqrt{\frac{2}{T}\left(d_0\tau_0 + d_1\frac{\tau_1}{1+\omega_1^2\tau_1^2}\right)}, \quad (19)$$

where $d_i = b_i/\sum_i b_i$. While a little more complicated when $\beta_i = 2$, the same method as outlined in Ref. [33] leads to a similar idealized error estimate.

In arriving at an ideal error there is also a parameter governing the steps skipped between successive boxes. It needs to be large enough that each box can be considered statistically independent. We used a sliding box method that skips roughly a $1/e$ step in time between sampled boxes. This avoids error effects that may arise due to correlations in short time evolution of the system, thus giving a more robust statistical sampling in a given simulation run. The fits allow us to use smaller t_w, which avoids sampling statistical fluctuations prevalent in the late time behavior of the ACFs. This then allows us to have a shorter T_{traj}.

III. RESULTS AND DISCUSSION

A. Diffusive properties of strongly correlated systems

Diffusive properties can be difficult to understand in a highly correlated plasma. However, results from dense liquid studies [31] provide a tool for understanding how the correlations manifest in the VACF. A consistent interpretation is found by using the $g(r)$ as an indicator of the existence of these correlations and then fitting using the appropriate functional form. As discussed in the Appendix, the coupling term depends on the location of the peak in $g(r)$.

In order to get statistically converged results for diffusive properties using the standard error in Eq. (14), one can run the simulation to very long T_{traj} (as done in Ref. [12]), increase particle number N, or both. When the value of Γ is large, it is very instructive to look at both the $g(r)$ and the VACF instead of just numerically integrating the VACF. There is much information to be gleaned by investigating the structural properties of the VACF [31]. In cases where glassy or solid-like behavior is setting in, secondary time scales emerge, which make using a single exponential function inadequate, e.g., studies near the triple point of water [35].

To study the emergence of structure in the VACF, we will analyze two systems at a fixed temperature and varying densities. For the case of Cu we use 54 ions at $T = 100$ eV and densities 1, 10, 30, and 67.4 g/cm^3. The final density is that used in Ref. [12]. Our smallest time step is 7 a.u. (where 1 a.u. corresponds to 0.024 fs) in the highest density simulation. For the case of CH, we use 24 C and 30 H ions at $T = 10$ eV and densities 1, 4, 8, 12, and 16 g/cm^3. Our smallest time step was 0.80 a.u. In a mixture, it is difficult to get particle number statistics and large T_{traj}. Thus, having a fitting routine based on the physics of the interactions is essential for determining accurate transport parameters.

1. Copper

In Fig. 1, we show fits to the VACF for Cu at $\rho = 67.4$ g/cm^3 as well as the numerically integrated results. Using Eq. (10), we fit the numerical data in the top panel in Fig. 1. The solid, light-red line goes smoothly through the data points. Both the fit to the VACF and its analytic integral yield results for Cu diffusion, which are in statistical agreement with each other using the standard error in Eq. (16). Additionally, both values are within the error bars associated with the method used in Ref. [12]. We also calculate the error in the fit using the covariance matrix of the fit parameters.

We also include an example of the fit using a single exponential (the solid black line), which is done by setting $a_i \equiv 0\ \forall\ i > 0$. The values for D_{exp} extracted from fitting to the VACF and its integral are statistically different. In the top panel, the single exponential tends to zero quickly and in so doing, settles on an intermediate time scale for decay yielding a 16% smaller D. However, in the bottom panel we note that the agreement between the more complex fit and the single exponential is good given that the exponential tends to the same long-time limit (dashed lines). The difference between the single-exponential decay times in the top and bottom panels is another indicator that necessary physics has not been included. We give the values of the parameters and their associated total error in Table I. Constrained parameters are not given an error bar. The total error in the diffusion constant is the sum of the statistical and fit errors. The adjusted $\bar{R}^2$ value for the exponential fit is 0.95 while it is 0.999 for the fit using Eq. (10). This is a small difference in the quality of the fit.

Another way to understand the onset of structure is to examine the PDF in Fig. 2(a). This PDF is indicative of a correlated liquid because peaks and valleys emerge as the density is increased. At $\rho = 67.4$ g/cm^3, the Cu ions have a

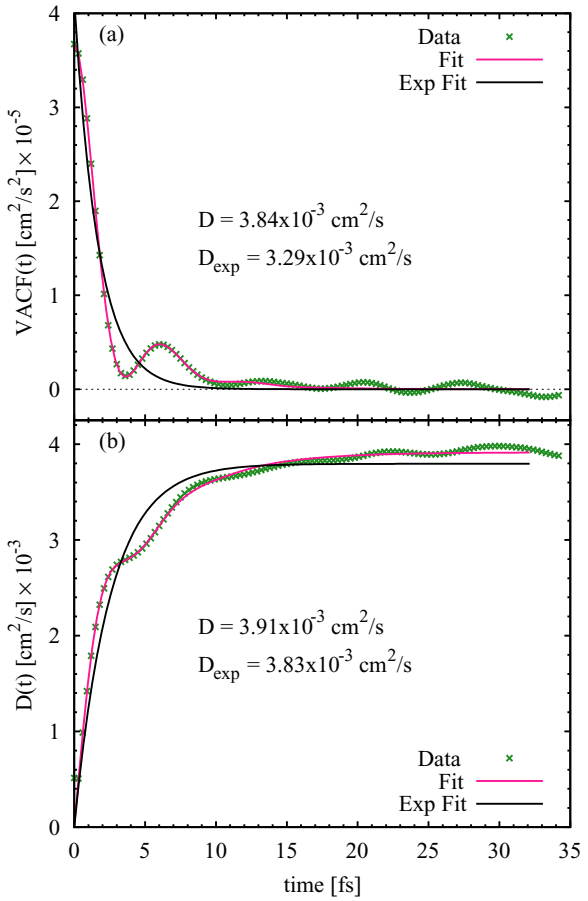

FIG. 1. (Color online) Computer-generated data from an OFMD run on Cu at $T = 100$ eV and $\rho = 67.4$ g/cm^3. (a) The green "x" are the numerical data, while the light-red solid line is the fit to Eq. (10). (b) The numerically integrated data represented by green "x" and the fit to the analytic integral of Eq. (10) is the light-red solid line. In both panels, the solid black line is the example of a single exponential fit, which is given by $a_i \equiv 0 \; \forall \; i > 0$.

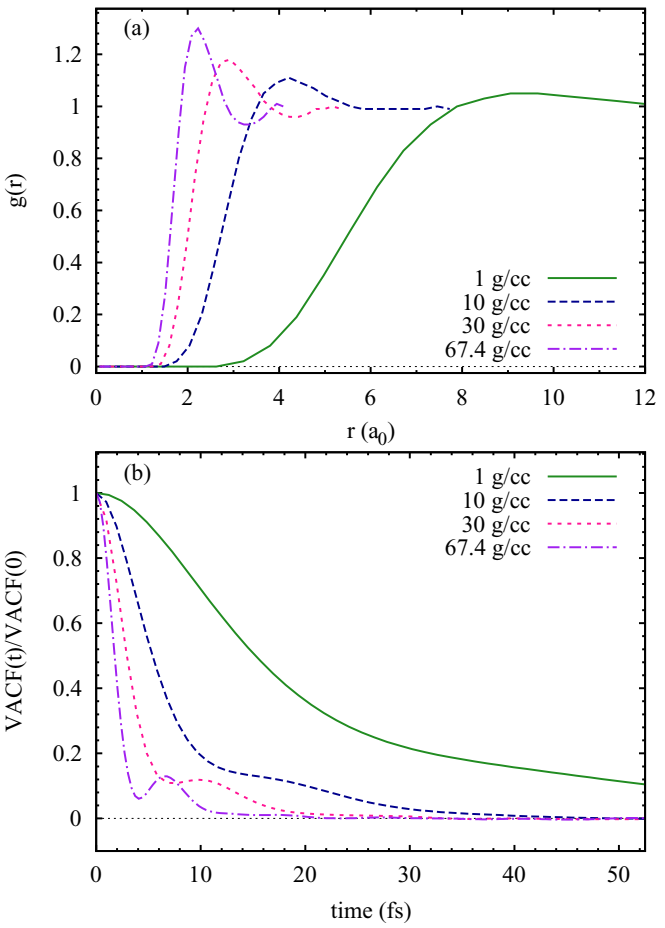

FIG. 2. (Color online) (a) Pair correlation function for Cu at $T = 100$ eV at various densities. The strong peak around $r = 2.2a_0$ is indicative of transient, collective motion. It is this correlation that gives rise to structure in the VACF. (b) The VACF for various densities of 1 (solid green), 10 (dashed purple), 30 (dotted light-red), and 67.4 (dash-dot violet) g/cm^3, and all are at $T = 10$ eV. There is a clear emergence of structure as the density goes up.

tendency to be around $2.2a_0$ from one another. The narrowing of the peak as density increases is a tell-tale sign of correlated behavior becoming more important.

In Fig. 2(b) we study the impact on the VACF of varying the density in Cu. Clearly there is structure as the density is increased. Even at the lowest density, evidence of a secondary time scale exists, though weakly. As the density increases a plateau forms in the VACF, which indicates a restorative force is causing the Cu ions to diffuse in a nonexponential manner. This can be understood on the basis of the itinerant oscillator model put forth by Sears [14] and expanded in Ref. [15]. The ion interacts with the medium around it. When the medium is diffuse, there is less interaction and thus a smaller restoring force, hence a single exponential is adequate for lower densities. As the density increases so does the influence of the medium on the ion, and the restorative force that acts on the ion increases or stiffens. We see this since ω_1 grows with increasing density. The values of τ_i and ω_i can be found in Table II along with our T_{traj} for each system. We also include the relative weights (the c_i) values.

To properly analyze the VACF we need to use a t_w, which is larger than our decay times τ_i but vastly smaller than our T_{traj}. If instead we try to use a large t_w to find a one-σ spread, as

TABLE I. Parameters given in the fits to the VACF in Eq. (12) for Cu at $T = 100$ eV and $\rho = 67.4$ g/cm^3. We also include the exponential (Exp.) fit results, which have $a_i \equiv 0 \; \forall \; i > 0$. The error includes both statistical error according to Eq. (16) as well as errors associated with each parameter via standard propagation of errors techniques.

Method	a_0(cm^2/s^2)×10^{-5}	τ_0 (fs)	a_1(cm^2/s^2)×10^{-5}	τ_1 (fs)	ω_1 (fs^{-1})	α_1	D (cm^2/s)×10^{-3}
Eq. (12)	1.70 ± 0.04	3.80 ± 0.07	1.97	2.44 ± 0.04	0.998 ± 0.006	0.64	3.84 ± 0.04
Exp.	4.1 ± 0.1	1.7 ± 0.1					3.29 ± 0.12

TABLE II. The values of the decay times and restorative frequencies in Cu as a function of density at $T = 100$ eV. We get the value of D from Eq. (12). The diffusion error is the sum of both statistical and fit contributions.

ρ (g/cm^3)	c_0	c_1	τ_0 (fs)	τ_1 (fs)	ω_1 (fs^{-1})	D (cm^2/s)$\times 10^{-3}$	T_{traj} (ps)
1	0.790 ± 0.004	0.210 ± 0.004	22.5 ± 0.1	9.8 ± 0.1	0.148 ± 0.001	34.7 ± 0.3	7.54
10	0.682 ± 0.007	0.318 ± 0.007	8.7 ± 0.1	4.52 ± 0.05	0.335 ± 0.003	12.1 ± 0.2	11.7
30	0.563 ± 0.008	0.437 ± 0.008	5.5 ± 0.1	3.08 ± 0.05	0.635 ± 0.001	6.61 ± 0.15	7.03
67.4	0.462 ± 0.011	0.558 ± 0.011	3.8 ± 0.1	2.44 ± 0.07	0.994 ± 0.002	3.85 ± 0.15	60.4

done in Ref. [12], we would find it computationally prohibitive to study lower density systems. As the density decreases, the decay times increase requiring an even larger t_w, which means even longer simulations. A factor of 10 increase in the decay times τ would require ten times as many steps to reach the same statistical convergence. We conclude that the simulations in Ref. [12] would require around 60 000 time steps at lower densities. While feasible, it is not advantageous to pursue for mixed-species systems where each time step is computationally expensive.

In our simulations of Cu, we had a time skip of τ between boxes. This was to prevent errors from correlations in the evolution of the system from creeping in. In Ref. [12] (Fig. 3) it is unclear whether they skipped any steps between successive boxes. However, given that their t_w is about half their T_{traj}, there cannot be many boxes in total. Hence, they see a spread that grows roughly as $\sqrt{t_w/T_{\text{traj}}}$. There is a prevalence of fluctuations above their diffusion average line that could be a consequence of this correlated evolution.

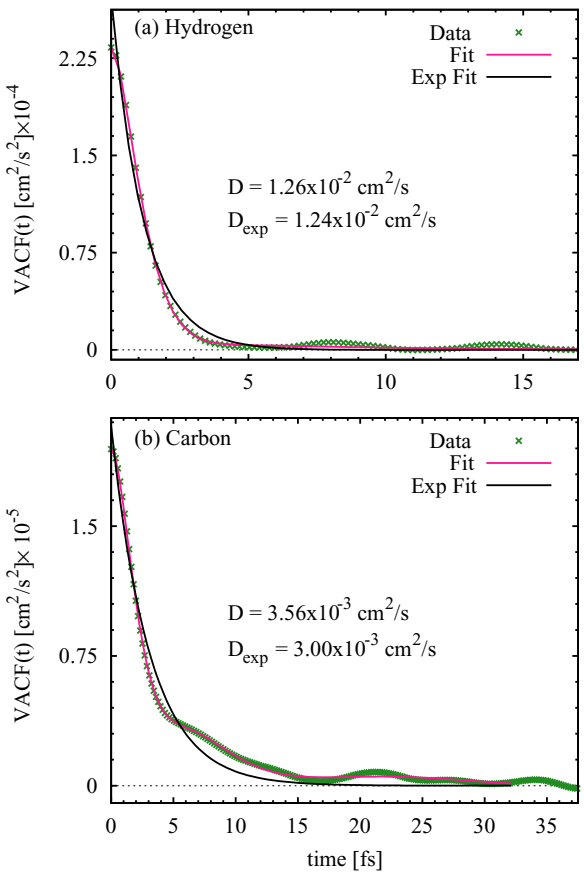

FIG. 3. (Color online) (a) VACF for C in the CH mixture using Eq. (12) with $i = 2$, and (b) VACF for H in the CH mixture using Eq. (10). The green "x" marks are the simulation data, and solid light-red line is the fits using the respective equations. The solid black line is the single exponential fit, $a_i \equiv 0 \,\forall\, i > 0$ in Eq. (12).

To test the ability of the fitting procedure to save computational resources, we reduce the number of time steps sampled and reanalyze the VACF. We are able to get statistically similar diffusion coefficients with only 750 steps (reduced from 22 000) with error increasing from 1% to 5%. A more stringent test of this method is with viscosity, as discussed below.

2. *Carbon-hydrogen mixture*

In Fig. 3(b) we give the VACF and its fits from the simulation for carbon at 16 g/cm^3 and $T = 10$ eV. The C VACF shows structure and evidence of a secondary restoring force, which if included gives a better fit via the $\bar{R}^2$ criteria. Mixtures offer more complexity and therefore require more care in analyzing the simulation data. In Fig. 3(a) we show the VACF for the hydrogen atom in the CH mixture; where slight evidence of structure exists. We need to only include the C-H restoring force because the H-H interactions are weak. However, in both H and C it is clear that a single exponential model ($a_i \equiv 0 \,\forall\, i > 0$) is insufficient to correctly describe the diffusive motion. There are clearly different time scales and structure appearing in the same simulation.

Additionally, we fit the integral of Eq. (10) to compare the two methods. We find that the integrated fits yield very similar time constants τ_i and restoring frequencies ω_i as the VACF fits. This provides a check on our fitting methods.

In the fits we also include an example of a single exponential ($a_i \equiv 0 \,\forall\, i > 0$), given by the solid black line in Fig. 3. The value of D_{exp} for Hydrogen is comparable and within statistical and fitting noise of the fit using Eq. (12) with $i = 1$. However, for carbon diffusion, the value of D_{exp} is smaller than that of the fit using Eq. (12) with $i = 2$ by about 16%. This emphasizes that a single exponential can be sufficient for one component in a mixture but not the other. Details of the fit can be found in Table III.

We also ran simulations on the CH mixture at different densities. This illustrates the onset of structure as we go to higher densities, where correlated motion is likely to emerge. In Fig. 4 we present the normalized VACF for H and C (Figs. 4(a) and 4(b), respectively). At low densities the VACF is a simple exponential. As the density increases a bump begins to form, indicating structure in both H and C VACFs. Again, as the density is increased we see a stiffening of the ω_i. We give the values of the ω_i in Table IV. Densities less than 8 g/cm^3 have ω_i that are effectively zero.

TABLE III. Parameters given in the fits to the VACF in Eq. (12) that lead to the diffusion constant as given in Eq. (6) for C and H ions in a near equal mixture of CH. For C we need to use a_1 and a_2 terms to get a better fit and reduce the overall fitting error.

Species	Method	a_0(cm^2/s^2)$\times 10^{-5}$	τ_0 (fs)	a_i(cm^2/s^2)$\times 10^{-5}$	τ_i (fs)	ω_i (fs^{-1})	α_i	D (cm^2/s)$\times 10^{-3}$
H	Eq. (12)	1.2 ± 0.1	4.8 ± 0.3	22.2 ± 0.1	0.86 ± 0.01	0.63 ± 0.01	1.88 ± 0.07	14.6 ± 0.4
H	Exp.	27.4 ± 0.3	1.28 ± 0.02					14.6 ± 0.3
C	Eq. (12)	0.73 ± 0.03	8.1 ± 0.2	1.10 ± 0.04	1.80 ± 0.04	0.64 ± 0.01	1.11 ± 0.04	3.4 ± 0.1
				0.10 ± 0.01	12.3 ± 0.8	0.26 ± 0.01	0.7 ± 0.2	
C	Exp.	2.08 ± 0.02	3.36 ± 0.04					2.9 ± 0.1

Because H is lighter than C, the diffusion occurs on a shorter time scale. The abscissa in Figs. 4(a) and 4(b) differ. We must use a larger t_w in the simulations to describe carbon diffusion, indicating that T_{traj} must be based on time scales associated with C diffusion, not H.

For the CH mixture we again test the fitting procedure as a means to save computational resources. We are able to get statistically similar diffusion coefficients for C with only 2×10^4 steps (down from 4×10^4) with error of about 4% error. If the number of steps is reduced further, the fit becomes more inaccurate and dominates the error estimates. The issue is that we still have to propagate the system on the light mass time scale but evolve long enough for the heavy mass time scale to extract C results.

At the lowest densities, the diffusion for both H and C atoms is exponential as with Cu. As the density increases, a single exponential begins to fail. However, the density at which it fails for H is higher than that for C. Different species within a mixture can have different physically motivated VACFs. Thus, we have to include the appropriate physics for each species and not enforce the physics in the model onto a system that is not exhibiting a specific behavior. Recall that $\Gamma_{CC} > \Gamma_{HC} > \Gamma_{HH}$, and thus we expect C ions to experience restoring forces due to correlated motion before H ions as density is increased.

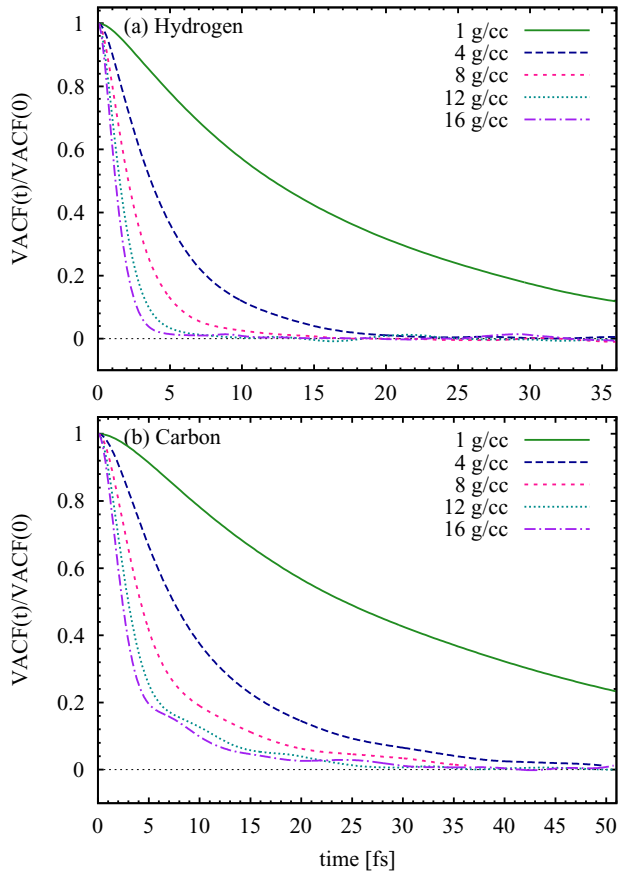

FIG. 4. (Color online) VACF for H (a) and C (b) for densities 1 (solid green), 4 (dash purple), 8 (short-dash light-red), 12 (dotted light-blue), and 16 (dash-dot violet) g/cm^3, all at $T = 10$ eV.

In Fig. 5 we have plotted the VACF as a function of time rescaled by τ_0. This places the ACFs on the same scale highlighting clearly that a single exponential works at low density but fails at high density.

We note that in Fig. 5(b) the limit seems to be above the simulation data, indicating that D has been over-estimated. However, there are fluctuations about zero in the VACF for low density, shown in Fig. 5(a). If we extend the viewing window, we find that the integrated value also fluctuates about the limit of the fit. This is why we want to fit with a smaller t_w as we vastly improve the counting statistics and do not have to run for restrictively long T_{traj}.

Had we insisted on an exponential fit, we would have used a value of t_w that is longer than the longest time scale in the problem. Using a longer t_w implies using a longer T_{traj}. For example, if we increase t_w by a factor of 2, then to reach the same level of statistical accuracy would require us to double T_{traj}. However, by using the more complex fit, which accounts for the physics, we have a window which meets the criteria in Eq. (15).

B. Viscosity in strongly correlated systems

Viscosity is a more challenging property to extract from OFMD simulations due to the global nature of the stress tensor. Increasing particle number does not reduce the statistical error, only increasing T_{traj} does. In addition, when there are two time scales involved one needs to run the simulation such that $T_{traj} \gg t_w$, which has to satisfy Eq. (15). Therefore, when computational time is a premium, robust fitting routines allow for shorter T_{traj} without diminishing the quality of the viscosity extracted.

We use Eq. (17) with fixed β_i. Some studies allow the β_i to vary [34] while others keep them fixed [35]. Physically, β controls how quickly the system relaxes to $1/e$. In the limit $\beta \to 0$ the system instantaneously relaxes to $1/e$ and then remains unrelaxed at this value. Ref. [34] hinted that this might be an example of an ideal glass transition. The other limit of $\beta \to \infty$ represents a system that suddenly relaxes to $1/e$ completely after a time τ but stays at this value infinitely long. We fix $\beta_1 = 1$ in all examples to keep the integral of Eq. (17)

TABLE IV. The values of the restorative frequencies in CH as a function of density. Below 8.0 g/cm^3 the ω_i are zero.

ρ g/cm^3	ω_1(H) (fs^{-1})	ω_1(C) (fs^{-1})	ω_2(C) (fs^{-1})	D_{H} (cm^2/s)$\times 10^{-2}$	D_{C} (cm^2/s)$\times 10^{-3}$
8.0	0	0.24 ± 0.1	0	26.3 ± 0.4	5.6 ± 0.1
12.0	0.49 ± 0.05	0.65 ± 0.01	0	17.9 ± 0.6	3.9 ± 0.2
16.0	0.63 ± 0.01	0.64 ± 0.01	0.26 ± 0.01	14.6 ± 0.4	3.4 ± 0.1

simple. For β_0 we use either 1 or 2, whichever yields a better fit.

1. Copper

In Fig. 6 we present both the STACF and the numerically integrated STACF. The solid lines are fits using Eq. (17) and its integral with $\beta_0 = 2$ and $\beta_1 = 1$. The simulation data beyond about 18 fs oscillates about zero in the STACF and therefore about the final viscosity value in the integrated data. Fitting over the whole range samples the large random walks that the simulation takes around the true value of η, thus distorting it. Both the fit to the STACF and its integrated form yield values of η that are in statistical agreement with each other as well as within the error quoted in Ref. [12].

In using Eq. (17) to fit the STACF we have to account for the fitting error as well as the statistical error. The fit is not as robust as in the case Eq. (12). We find that the STACF simulation data yield $\eta = 39.8 \pm 1.3$ mPa s. The analytic fit to the integrated simulation data yields $\eta = 40.6 \pm 5.8$ mPa s. The fit to the integrated data is noisier given the fluctuations about the limiting value to which the exponential functions are trying to reach. The Gaussian coefficient b_0 is much larger than the exponential, indicating its importance in the fit.

To test the ability of the fitting procedure to save computational resources, we reduce the number of time steps sampled

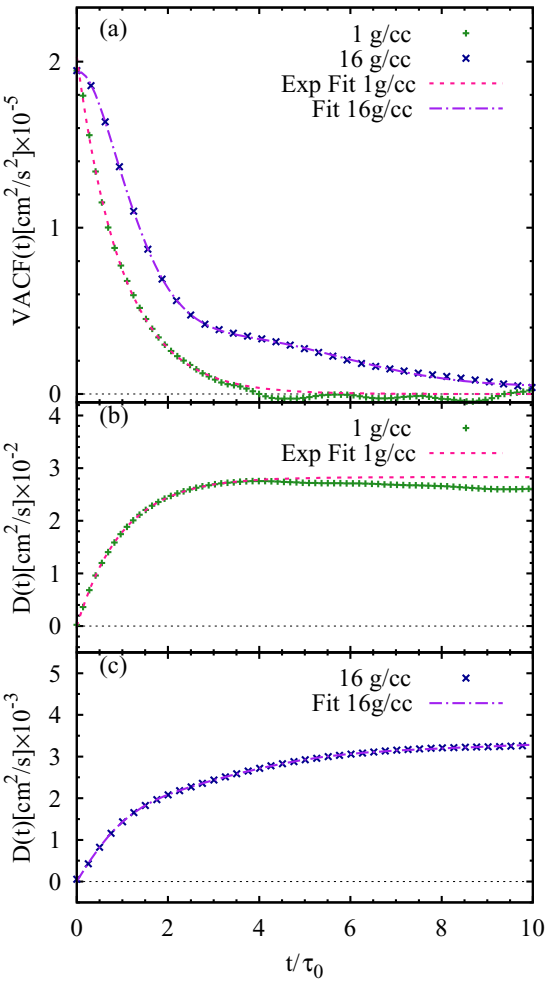

FIG. 5. (Color online) (a) VACF for H in CH at 1 and 16 g/cm^3. $\tau_0^{1g/cc} = 33.6$ fs and $\tau_0^{16g/cc} = 12.6$ fs. In (b) and (c) we plot the integrated value and fit of the 1 and 16 g/cm^3 simulation, respectively. The 16 g/cm^3 fit is to Eq. (12) with $i = 1$ while 1 g/cm^3 is a fit to Eq. (12) with $a_i \equiv 0 \,\forall\, i > 0$.

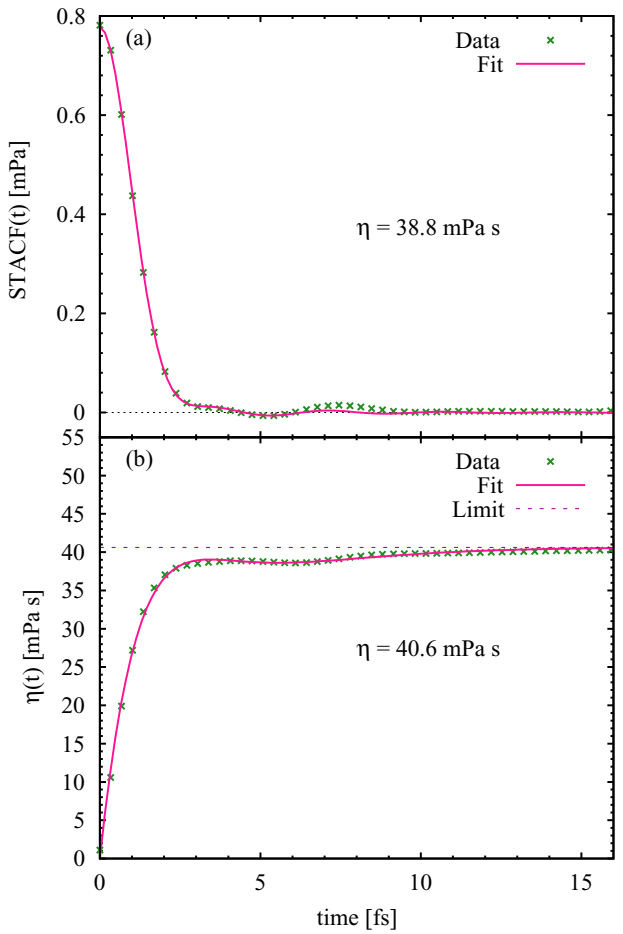

FIG. 6. (Color online) The STACF for Cu at $T = 100$ eV and $\rho = 67.4$ g/cm^3. (a) The STACF simulation data (denoted by a green "x") and the solid light-red line is the fit using Eq. (17). (b) The numerically integrated simulation data with the fit (solid light-red line) the fit to the analytic integral of Eq. (17). The two values obtained are statistically the same.

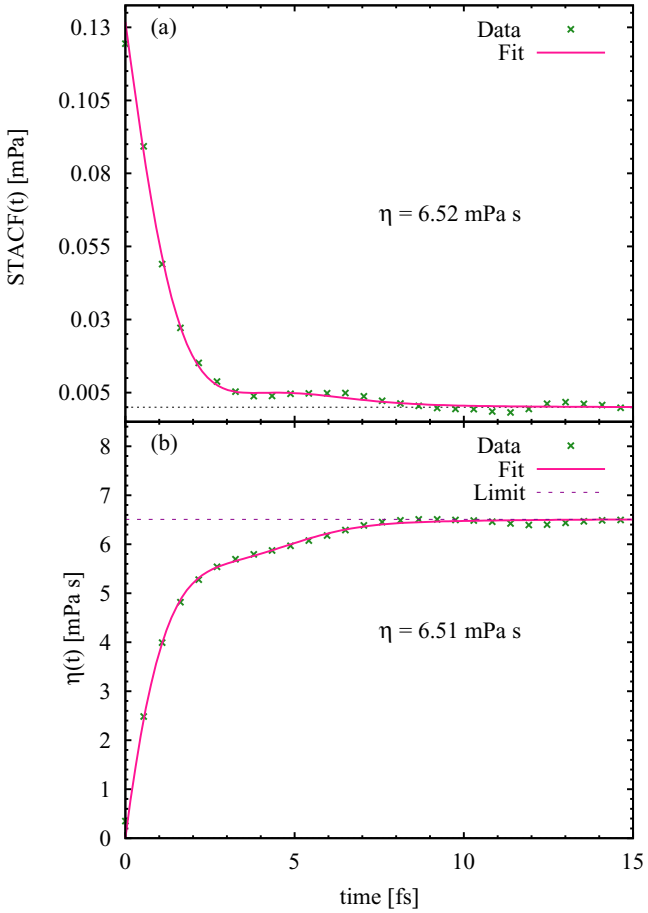

FIG. 7. (Color online) (a) STACF simulation data and (b) numerical integral (given by green "x") for the CH system at $T = 10$ eV and $\rho = 16$ g/cm^3. The fits are to Eq. (17) and its analytic integral. The numbers are statistically the same.

and reanalyze the STACF. We are able to get statistically similar viscosity with only 750 steps (reduced from 22 000) with error increasing from 2% to 10%. For 5% error, we need about 5 000 steps. Note this is the same simulation that produces the diffusion coefficients.

By using $10x$ fewer particles in their viscosity simulations as in the diffusion one, Ref. [12] ran the simulation for a factor of $10x$ longer. This strategy obfuscates the accuracy of the respective simulations, given that one benefits from the extra $1/\sqrt{N}$ reduction of error in self-diffusion and the other runs for a much longer T_{traj}. Additionally, by using such a large window size in their Fig. 10 they are subject to the random fluctuations associated with the statistical sampling. Perhaps this is why the authors used a smaller averaging window in viscosity compared to diffusion. The noise introduces too much error, and this is why a smaller t_{w} should be used as well as a fitting function.

2. *Carbon-hydrogen mixture*

In studying a mixture, using a fit is requisite given the computational demand due to the large number of particles needed for adequate statistics for each species. In Fig. 7 we show the STACF and its integrated value for the CH mixture. Solid lines are fits using Eq. (17) with both $\beta_i = 1$ and its integral. We are able to reduce the oscillations about zero in the STACF (top panel) and the final viscosity value (bottom panel) by using a smaller time window. This in turn allows the gathering of more statistics in the full simulation, which reduces the effects of random walks.

As in the case of Cu, the fitting routine is not as robust for viscosity. However, both the fit for the STACF and its analytic integral yield results that are in statistical agreement with each other. We find that $\eta = 6.5 \pm 1.7$ mPa s and $\eta = 6.5 \pm 1.3$ mPa s for the STACF and integrated STACF, respectively. The larger error bars are due primarily to the fitting error. This is largely due to the fluctuations in the STACF data at longer times. Without the $1/\sqrt{N}$ benefit, viscosity is a much tougher parameter to nail down. In examining the structure in the top panel of Fig. 7, we see clearly an increase in the STACF around $t = 3.6$ fs. A single exponential underestimates the value of viscosity unless we use a rather large t_{w}, which in turn reduces our statistics and confidence in the value because $\sqrt{t_{\text{w}}/T_{\text{traj}}}$ becomes larger.

The time scales associated with our fits in the CH viscous system are all comparable. At the highest density, the oscillatory term becomes very important in the fit. Without it, we would not correctly describe the system. Note that if there is considerable noise in the system, extracting ω can be fruitless since the noise washes out any such frequency. Long T_{traj} are requisite to allow for better statistics. Thus, a simple two-exponential fit might be of better use if the oscillatory contributions are not overly pronounced.

As we reduce the density of the CH mixture, thus moving toward less correlated systems, we find that the time scale of τ_0 becomes longer, as does τ_1. However, the importance of τ_1 is many orders of magnitude below that of τ_0 given the weights d_i. d_0 increases with decreasing density while the d_1 decreases. This further emphasizes that a single exponential captures the essential physics at lower densities, or more aptly, for systems where $\Gamma_{ij} < 1$. In such systems the correlations are much smaller as there is less structure.

Once again we look at how the fitting procedure can be used to save computational time, this time for the CH viscosity. This is the most costly set of simulations we ran. For the full simulation, we used 4×10^4 time steps, which resulted in error of about 14%. We can use the fitting procedure and run 2×10^4 steps to 17% error. Once again further reducing the number of time steps used in the analysis the fit error becomes large.

IV. CONCLUSIONS

We have studied the behavior of correlated warm dense matter systems with OFMD simulations. We focused on extracting the diffusion and viscosity properties from ACFs. In the correlated regimes, the ACFs have structure and multiple time scales. Such behavior is anticipated in dense liquid theory [31], and interpreted using standard fitting forms. These fitting forms offer a means to include more physics in the functional form of the ACFs, thus allowing a reduced computational burden to determine the transport properties. In addition to looking at a strongly interacting single species system, we also looked at a CH mixture. Such a system implicitly has

multiple times scales since the lighter protons (H) move more quickly than the heavier carbon ions.

We further studied the behavior of these systems as the density is varied from weakly interacting ($\Gamma < 1$) to strongly interacting ($\Gamma > 1$). We study how structure emerges as density is increased. The mixtures have a more complex behavior, where the C VACF behaves in a distinctly different manner than H over a wide parameter range.

We extended previous work [8] where either exponential or Gaussian fits to ACFs were used in the determination of transport properties. Such fits reduce the computational cost of an MD simulation significantly. One can use a shorter t_w, which allows for more statistical sampling of the trajectory and arrive at statistically and physically sound transport property. The original use of the fitting form in Ref. [8] was for weakly interacting systems ($\Gamma < 1$); i.e., hard sphere physics well-describes the interactions. In a more highly correlated system, this approximation is no longer applicable. For diffusion, we extended the formulation beyond the standard Enskog theory by including extra terms, which act on various time scales and a frequency associated with restorative forces in the system. For viscosity, we use a variation of the Kohlrausch law.

Future work will be to explore the temperature and density dependence of the mass transport parameters D and η of complex and correlated mixtures. For example, four component mixtures relevant to exoplanet systems, and systems of much greater mass imbalance, such as third-row metals paired with hydrogen, will be explored in the WDM regime.

ACKNOWLEDGMENTS

The authors acknowledge discussions with J. Clerouin and gratefully acknowledge support from the Advanced Simulation and Computing Program (ASC), science campaigns 1 and 4, and LANL, which is operated by LANS, LLC for the NNSA of the U.S. DOE under Contract No. DE-AC52-06NA25396.

APPENDIX: DERIVATION OF VAC FIT FORMS

We start with the itinerant oscillator model of Sears [14] as modified by Damle, Sjölander. and Singwi [15]. Instead of one fictitious center, we allow for two. This leads to the following set of coupled equations

$$\ddot{\boldsymbol{R}}_0[t] + \int_0^t \mu_0[t-t']\dot{\boldsymbol{R}}_0[t']dt' + \frac{\alpha_{01}^2}{M_0}(\boldsymbol{R}_0[t] - \boldsymbol{R}_1[t]) + \frac{\alpha_{02}^2}{M_0}(\boldsymbol{R}_0[t] - \boldsymbol{R}_2[t]) = \boldsymbol{F}_0[t], \tag{A1}$$

$$\ddot{\boldsymbol{R}}_1[t] + \int_0^t \mu_1[t-t']\dot{\boldsymbol{R}}_1[t']dt' + \frac{\alpha_{10}^2}{M_1}(\boldsymbol{R}_1[t] - \boldsymbol{R}_0[t]) + \frac{\alpha_{12}^2}{M_1}(\boldsymbol{R}_1[t] - \boldsymbol{R}_2[t]) = \boldsymbol{F}_1[t], \tag{A2}$$

$$\ddot{\boldsymbol{R}}_2[t] + \int_0^t \mu_2[t-t']\dot{\boldsymbol{R}}_2[t']dt' + \frac{\alpha_{20}^2}{M_2}(\boldsymbol{R}_2[t] - \boldsymbol{R}_0[t]) + \frac{\alpha_{21}^2}{M_2}(\boldsymbol{R}_2[t] - \boldsymbol{R}_1[t]) = \boldsymbol{F}_2[t], \tag{A3}$$

where the subscript 0 indicates the atom of interest, while 1 and 2 are the fictitious centers. We cast this into a more amenable matrix form (using $\dot{\boldsymbol{V}}[t] = \ddot{\boldsymbol{R}}[t]$):

$$\dot{\boldsymbol{V}} + \int_0^t \underline{\boldsymbol{\Gamma}}[t-t'] \cdot \boldsymbol{V}[t']\, dt' = \boldsymbol{F}[t]. \tag{A4}$$

We absorb the frequencies α_{ij} into the friction matrix $\underline{\boldsymbol{\Gamma}}$ and its form is given by

$$\underline{\boldsymbol{\Gamma}}[t] = \begin{pmatrix} \mu_0[t] + \omega_{01}^2 + \omega_{02}^2 & -\omega_{01}^2 & -\omega_{02}^2 \\ -\omega_{10}^2 & \mu_1[t] + \omega_{10}^2 + \omega_{12}^2 & -\omega_{12}^2 \\ -\omega_{20}^2 & -\omega_{21}^2 & \mu_2[t] + \omega_{20}^2 + \omega_{21}^2 \end{pmatrix}, \tag{A5}$$

where $\omega_{ij}^2 = \alpha_{ij}^2/M_i \neq \omega_{ji}^2$. Sears [14] gave an expression for ω_{ij}^2 in the case of one atom of interest in a sea of others. Here, the same ideas and methods can be applied to arrive at an expression for ω_{0i}^2,

$$\omega_{0i}^2 = \frac{4\pi N_i}{3m_i V}\int_0^\infty \left[\phi_{0i}''(a) + 2\frac{\phi_{0i}'(a)}{a}\right] g_{0i}(a)a^2 da, \tag{A6}$$

where $g_{0i}(a)$ is the pair correlation function, $\phi_{0i}(a)$ is the interaction potential, and N_i the number of particles of type i that the particle of interest (0) interacts. We note that in the screened Coulomb interaction this integral requires the screening length to be larger than where $g_{0i}(a)$ turns on and/or peaks, hence in a plasma regime where interactions are strong. In the case of molecular interactions when $g_{0i}(a)$ peaks at the minimum of the $\phi_{0i}(a)$ then we get out the molecular vibration constant. Thus, this method can be applied to the high pressure and temperature cores in planets such as Neptune and Uranus as well.

Using the methods in Ref. [15] and defining p as our Laplace space variable,

$$\underline{\boldsymbol{\phi}}[p] = [p\,\underline{\boldsymbol{I}} + \underline{\boldsymbol{\Gamma}}[p]]^{-1}\underline{\boldsymbol{\phi}}^0, \tag{A7}$$

$$\underline{\boldsymbol{\Gamma}}[p]\underline{\boldsymbol{\phi}}^0 = \underline{\boldsymbol{F}}[p], \tag{A8}$$

$$\phi_{ij}^0 = \delta_{ij}\frac{k_B T}{M_i}, \tag{A9}$$

where $\phi_i[p]$ and $\Gamma[p]$ are the Laplace transforms of $\langle \mathbf{V}_i[t] \cdot \mathbf{V}_i[0] \rangle$ and $\langle \mu_i[t] \mu_i[0] \rangle$, respectively. $\underline{\underline{I}}$ is the unit matrix. Equation (27) is the fluctuation-dissipation relation for this system. From here on out we will assume the centers do not interact with each other, which does not violate the fluctuation-dissipation relations. It merely amounts to setting $\omega_{21} = \omega_{12} = 0$.

After a bit of algebra we get to the following expression for the VAC of the particle of interest:

$$\phi_{00}[p] = \phi_{00}^0 \left\{ p + \mu_0[p] + \frac{\omega_{01}^2 (p + \mu_1[p])}{p (p + \mu_1[p]) + \omega_{10}^2} + \frac{\omega_{02}^2 (p + \mu_2[p])}{p (p + \mu_2[p]) + \omega_{20}^2} \right\}^{-1}. \tag{A10}$$

It is straightforward, though tedious, to find the N-center relation as well:

$$\phi_{00}[p] = \phi_{00}^0 \left\{ p + \mu_0[p] + \sum_{i=1}^{N} \frac{\omega_{0i}^2 (p + \mu_i[p])}{p (p + \mu_i[p]) + \omega_{i0}^2} \right\}^{-1}. \tag{A11}$$

We now split each $\mathbf{F}_i$ into two terms: a friction term and a restoring force term. The friction terms correspond to the $\mathbf{F}_i$ in Eq. (27), while the second term is the same for all and must adhere to Newton's third law. Thus,

$$\mathbf{F}_i[t] = \mathbf{A}_i[t] + \frac{\alpha}{M_i} \sqrt{3 k_B T} \mathbf{A}'. \tag{A12}$$

The $\mathbf{A}'$ satisfy the properties $\langle \mathbf{A}' \rangle = 0$ and $\langle \mathbf{A}' \cdot \mathbf{A}' \rangle = 1$. Then the fluctuation-dissipation relations yield

$$\frac{3 k_B T}{M_i} \mu_i[p] = A_i[p], \tag{A13}$$

with $A_i[p]$ the Laplace transform of $\langle \mathbf{A}_i[t] \cdot \mathbf{A}_i[0] \rangle$. The nondiagonal pieces of Eq. (27) tell us that $\langle \mathbf{A}_i[t] \cdot \mathbf{A}_j[0] \rangle = 0$ for $j \neq i$. The fluctuation-dissipation relation as well as Newton's third law tell us that $\omega_{ij}^2 \phi_{jj}^0 = \omega_{ji}^2 \phi_{ii}^0$.

We now assume that $\langle A_{i,\alpha}[t] \cdot A_{j,\beta}[0] \rangle = \delta_{ij} \delta_{\alpha\beta} \langle A_\alpha^2 \rangle \delta(t - t')$, and α and β are the Cartesian coordinates x, y, and z. This leads to

$$\mu_i[p] = \gamma_i, \tag{A14}$$

$$\gamma_i = \frac{M_i}{3 k_B T} \sum_\alpha \langle A_\alpha^2 \rangle. \tag{A15}$$

With this choice of correlation, we find the general form for $\phi_{00}[p]$ is

$$\frac{\phi_{00}[p]}{\phi_{00}^0} = \frac{\prod_{k=1}^{N} \left[p (p + \gamma_k) + \omega_{k0}^2 \right]}{\sum_{i=0}^{N} \left\{ \omega_{0i}^2 (p + \gamma_i) \prod_{k=1, k \neq i}^{N} \left[p (p + \gamma_k) + \omega_{k0}^2 \right] \right\}} = \frac{R[p]}{Q[p]}, \tag{A16}$$

and $\omega_{00}^2 = 1$. We see that we have a polynomial of order $2N$ in the numerator and of order $2N + 1$ in the denominator. Provided there are no shared roots between $R[p]$ and $Q[p]$, and that each root of $Q[p]$ is distinct, the general solution for $\phi[t]$ is

$$\frac{\phi[t]}{\phi_{00}^0} = \sum_\lambda \frac{R[p_\lambda]}{Q'[p_\lambda]} e^{p_\lambda t}, \tag{A17}$$

where p_λ are the roots of the polynomial $Q[p]$ and $Q'[p_\lambda]$ is the derivative of $Q[p]$ with respect to p evaluated at the roots p_λ.

In general, this is not a simple expression in time. However, if we let $\lambda_i = \sqrt{4\omega_{i0}^2 - \gamma_i^2}$ as well as make the approximation that ω_{0i} (not ω_{i0}) is small, then we find the much more tractable equation

$$\frac{\phi_{00}[p]}{\phi_{00}^0} \approx \frac{1}{(p + \gamma_0)} - \sum_{i=1}^{N} \omega_{0i}^2 \frac{p + \gamma_i}{(p + \gamma_0)^2} \frac{1}{\left(p + \frac{\gamma_i}{2}\right)^2 + \left(\frac{\lambda_i}{2}\right)^2}. \tag{A18}$$

Using standard relations for the inverse Laplace transform we arrive at

$$\frac{\phi_{00}[t]}{\phi_{00}^0} = e^{-t\gamma_0} \left[1 + \sum_{i=1}^{N} (\kappa_i + \delta_i t) \right] + \sum_{i=1}^{N} \chi_i e^{-\gamma_i t} \left(\mathrm{Cos}\left[t \lambda_i \right] + \alpha_i \mathrm{Sin}\left[t \lambda_i \right] \right), \tag{A19}$$

where κ_i, δ_i, χ_i, and α_i are complicated algebraic combinations of γ_0, γ_i, and λ_i. This is how we arrive at Eqs. (10) and (12), but we do not include the linear term in t. We exclude the linear term in t because it does not improve the adjusted R^2 value of the fit in the cases we studied. Using an exponential memory kernel, or a continued fraction approach, for the stochastic forces can also be done since it leads to the ratio of two polynomials with the denominator of higher order than the numerator. However, the complexity of the expressions gives neither a more meaningful nor more physical fitting function than Eq. (38).

[1] D. A. Hammel, S. W. Haan, D. S. Clark, M. J. Edwards, S. H. Langer, M. M. Marinak, M. V. Patel, J. D. Salmonson, and H. A. Scott, High Energy Density Phys. **6**, 171 (2010).

[2] K. Widmann, T. Ao, M. Foord, D. Price, A. Ellis, P. Springer, and A. Ng, Phys. Rev. Lett. **92**, 125002 (2004).

[3] M. Bethkenhagen, M. French, and R. Redmer, J. Chem. Phys. **138**, 234504 (2013).

[4] R. Chau, S. Hamel, and W. J. Nellis, Nat. Commun. **203**, 1198 (2010).

[5] T. Guillot, W. B. Hubbard, D. J. Stevenson, and D. Saumon, *Jupiter* (University of Arizona Press, Tuscon, 2003).

[6] N. C. Santos, W. Benz, and M. Mayor, Science **310**, 251 (2005).

[7] I. Kwon, J. D. Kress, and L. A. Collins, Phys. Rev. B **50**, 9118 (1994).

[8] D. A. Horner, F. Lambert, J. D. Kress, and L. A. Collins, Phys. Rev. B **80**, 024305 (2009).
[9] J. D. Kress, J. S. Cohen, D. P. Kilcrease, D. A. Horner, and L. A. Collins, Phys. Rev. E **83**, 026404 (2011).
[10] J. P. Hansen and I. R. McDonald, *Theory of Simple Liquids* (Elsevier, New York, 2006).
[11] D. A. McQuarrie, *Statistical Mechanics* (University Science Books, Herndon, VA, 2000).
[12] J.-F. Danel, L. Kazandjian, and G. Zérah, Phys. Rev. E **85**, 066701 (2012).
[13] J. G. Clérouin, M. H. Cherfi, and G. Zérah, Europhys. Lett. **42**, 37 (1998).
[14] V. F. Sears, Proc. Phys. Soc. **86**, 953 (1965).
[15] P. Damle, A. Sjölander, and K. S. Singwi, Phys. Rev. **165**, 277 (1968).
[16] F. Lambert and V. Recoules, Phys. Rev. E **86**, 026405 (2012).
[17] L. Burakovsky, C. Ticknor, J. D. Kress, L. A. Collins, and F. Lambert, Phys. Rev. E **87**, 023104 (2013).
[18] P. Arnault, High Energy Density Phys. **9**, 711 (2013).
[19] F. Lambert, J. Clérouin, J.-F. Danel, L. Kazandjian, and G. Zérah, Phys. Rev. E **77**, 026402 (2008).
[20] M. Brack and P. K. Bhaduri, *Semiclassical Physics* (Westview Press, Boulder, CO, 2003).
[21] J. P. Perdew and A. Zunger, Phys. Rev. B **23**, 5048 (1981).
[22] G. Fassurier, P. L. Silvestrelli, and C. Blancard, High Energy Density Phys. **5**, 74 (2009).
[23] F. Perrot, Phys. Rev. A **20**, 586 (1979).
[24] J. Clerouin, E. L. Pollock, and G. Zerah, Phys. Rev. A **46**, 5130 (1992).
[25] N. Troullier and J. L. Martins, Phys. Rev. B **43**, 1993 (1991).
[26] F. Lambert, J. Clérouin, and G. Zérah, Phys. Rev. E **73**, 016403 (2006).
[27] P. Minary, G. J. Martyna, and M. E. Tuckerman, J. Chem. Phys. **118**, 2510 (2003).
[28] M. P. Allen and D. J. Tildesley, *Computer Simulations of Liquids* (Oxford University Press, Oxford, 2006).
[29] M. Schoen and C. Hoheisel, Mol. Phys. **52**, 33 (1984).
[30] D. Alfe and M. J. Gillian, Phys. Rev. Lett. **81**, 5161 (1998).
[31] J. P. Boon and S. Yip, *Molecular Hydrodynamics* (Dover Publications, Mineola, NY, 1980).
[32] H. Mori, Prog. Theoret. Phys. **34**, 399 (1965).
[33] B. Hess, J. Chem. Phys. **116**, 209 (2002).
[34] G.-J. Guo, Y.-G. Zhang, K. Refson, and Y.-J. Zhao, Mol. Phys. **100**, 2617 (2002).
[35] D. Levesque, L. Verlet, and J. Kürkijarvi, Phys. Rev. A **7**, 1690 (1973).